

The dynamical origin of the universality classes of spatiotemporal intermittency

Zahera Jabeen

*Institute of Mathematical Sciences, Chennai, India.**

Neelima Gupte

Department of Physics, Indian Institute of Technology - Madras, Chennai, India[†]

(Dated: November 8, 2018)

Abstract

Studies of the phase diagram of the coupled sine circle map lattice have identified the presence of two distinct universality classes of spatiotemporal intermittency viz. spatiotemporal intermittency of the directed percolation class with a complete set of directed percolation exponents, and spatial intermittency which does not belong to this class. We show that these two types of behavior are special cases of a spreading regime where each site can infect its neighbors permitting an initial disturbance to spread, and a non-spreading regime where no infection is possible, with the two regimes being separated by a line, the infection line. The coupled map lattice can be mapped on to an equivalent cellular automaton which shows a transition from a probabilistic cellular automaton to a deterministic cellular automaton at the infection line. The origins of the spreading-non-spreading transition in the coupled map lattice, as well as the probabilistic to deterministic transition in the cellular automaton lie in a dynamical phenomenon, an attractor-widening crisis at the infection line. Indications of unstable dimension variability are seen in the neighborhood of the infection line. This may provide useful pointers to the spreading behavior seen in other extended systems.

PACS numbers: 05.45.-a, 05.45.Ra, 64.60.ah, 05.10.Gg

Keywords: Spatiotemporal intermittency, Directed Percolation, Cellular automaton, Crisis, Unstable Dimension Variability

*Electronic address: zahera@imsc.res.in

[†]Electronic address: gupte@physics.iitm.ac.in

I. INTRODUCTION

The identification of the universality class of spatiotemporal intermittency [1] in spatially extended systems has been a long standing problem in the literature. Early conjectures argued that the transition to spatiotemporal intermittency is a second order phase transition, and the transition falls in the same universality class as directed percolation [2]. This conjecture has become the central issue in a long-standing debate [3, 4, 5, 6, 7, 8], which is still not completely resolved.

Studies of the coupled sine circle map lattice have thrown up a number of intriguing observations of relevance to this problem [9, 10, 11]. This system has regimes of spatiotemporal intermittency (STI) with critical exponents which fall in the same universality class as directed percolation(DP), as well as regimes of spatial intermittency (SI) which do not belong to the DP class. Both these regimes lie on the bifurcation boundaries of the spatiotemporally fixed point solutions of the map. The spatiotemporally intermittent regime seen here has an absorbing laminar state, i.e. a laminar site remains laminar unless infected by a neighboring turbulent site. The burst states spread and can percolate through the entire lattice. The system shows a convincing set of DP exponents in this regime [9, 10, 11]. In the spatially intermittent regime, the laminar sites are frozen in time and the burst sites show temporally periodic or quasi-periodic behavior. The laminar sites do not get infected by neighboring turbulent sites. Hence, the spatially intermittent state is non-spreading and does not show DP exponents. Thus, both DP and non-DP behavior can be seen for different parameter regimes of the same system.

In the present paper, we show that the infective DP behavior of spatiotemporal intermittency and the non-infective behavior of spatial intermittency are special cases of the more general spreading to non-spreading transition seen in this system. The spreading and non-spreading regimes are separated by a line which we call the infection line. Above the infection line, the burst states can infect neighboring laminar states and spread through the lattice, whereas below this line the burst states cannot infect their neighbors and the non-spreading regime is seen. The infection line intersects the bifurcation boundary of the synchronized solutions. Intermittent solutions are seen along this boundary, with the DP type of STI being seen above the infection line, and the non-DP SI being seen below the infection line. Spreading and non-spreading solutions are also seen off the bifurcation boundary. However,

the distribution of laminar lengths shows power-law scaling only for parameter values which are very close to the bifurcation boundary, and falls off exponentially as the parameter values get more distant from the bifurcation boundary. Other exponents associated with DP behavior are also observed only along the bifurcation boundaries.

Further insights into the spreading to non-spreading transition are obtained by mapping the coupled map lattice (CML) onto a cellular automaton (CA). The spreading to non-spreading transition seen across the infection line maps on to a transition from a probabilistic cellular automaton to a deterministic cellular automaton. The dynamical origins of this transition lie in an attractor widening crisis which occurs at the infection line. The existence of this crisis can be inferred from the bifurcation diagram of the system. The finite-time Lyapunov exponents of the system fluctuate in the neighborhood of the infection line indicating the presence of unstable dimension variability. Thus the statistical characterizers of the system show signatures of a dynamical phenomenon. This result could have implications in a wider context.

The paper is organized as follows. In section II, we give details of the coupled sine circle map lattice and the associated phase diagram and discuss the special behavior near the bifurcation boundary in these two regimes, namely spatiotemporal intermittency and spatial intermittency seen in the spreading and non-spreading regimes respectively. The signatures of the spreading and non-spreading regimes are also seen in the mapping of the coupled map lattice to a cellular automaton and its mean-field analysis. This is discussed in section III. In section IV, we discuss the dynamic origins of the two regimes, namely, the presence of an attractor-widening crisis and unstable dimension variability, as indicated by the fluctuating Lyapunov exponents at the infection line. We conclude with a discussion of the implications of our results.

II. THE MODEL AND THE UNIVERSALITY CLASSES

The coupled sine circle map lattice studied here is known to model the mode-locking behavior [12] seen in coupled oscillators, Josephson Junction arrays etc. The model is defined by the evolution equation

$$x_i^{t+1} = (1 - \epsilon)f(x_i^t) + \frac{\epsilon}{2}[f(x_{i-1}^t) + f(x_{i+1}^t)] \pmod{1} \quad (1)$$

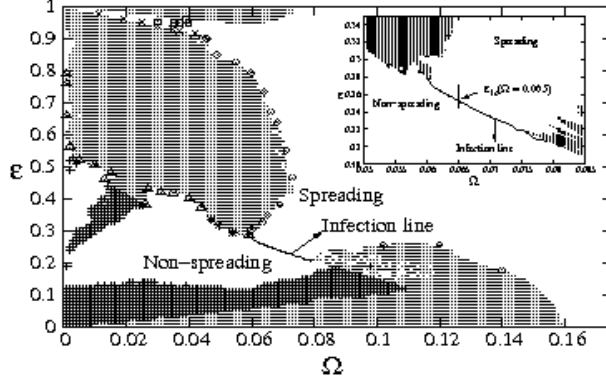


FIG. 1: shows the phase diagram of the coupled sine circle map lattice obtained with random initial conditions. The spreading and non-spreading regimes, separated by the infection line have been marked. Spatiotemporal intermittency of the directed percolation class is indicated by diamonds (\diamond), whereas spatial intermittency has been marked with asterisks ($*$) and triangles (\triangle).

where i and t are the discrete site and time indices respectively and ϵ is the strength of the coupling between the site i and its two nearest neighbors. The local on-site map, $f(x)$ is the sine circle map defined as $f(x) = x + \Omega - \frac{K}{2\pi} \sin(2\pi x)$, where, K is the strength of the nonlinearity and Ω is the winding number of the single sine circle map in the absence of the nonlinearity. We study the system with periodic boundary conditions in the parameter regime $0 < \Omega < \frac{1}{2\pi}$ (where the single circle map has temporal period 1 solutions), $0 < \epsilon < 1$ and $K = 1.0$. The phase diagram of this model evolved with random initial conditions is shown in Fig. 1.

Spatiotemporally fixed point solutions, in which all the sites relax to the fixed point $x^* = \frac{1}{2\pi} \sin^{-1}(\frac{2\pi\Omega}{K})$, are seen in a large region of the phase diagram, and are indicated by dots. Two distinct regimes, separated by a line, which we call the infection line, can be identified in the phase diagram. A spreading regime is seen above the infection line, in which the burst states can infect their neighboring laminar states and spread through the lattice. The spreading nature of the bursts is strongly evident when a disturbance introduced in a laminar background eventually spreads to the entire lattice by infecting the neighboring laminar sites (Fig. 2(a)). This is in contrast to the non-spreading regime seen below the infection line, where the random initial conditions die down to bursts which are localized, and do not infect their neighboring laminar states (Fig. 2(b)).

In both these regions, spatiotemporal intermittency with co-existing laminar states ex-

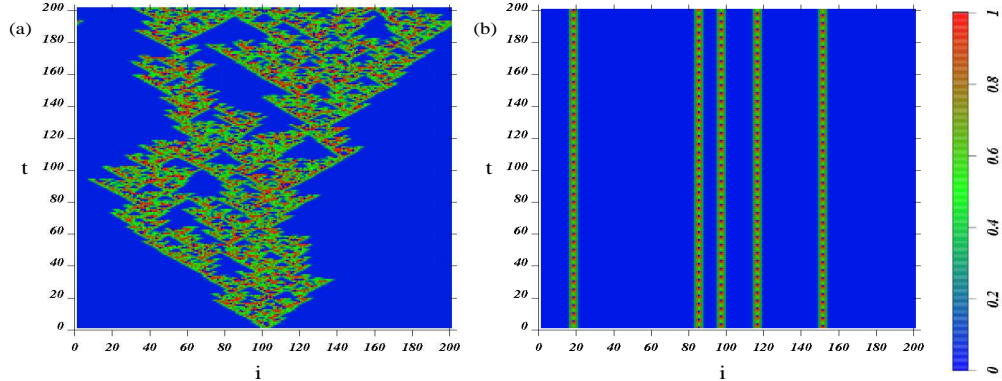


FIG. 2: (Color online) shows the space-time plot of (a) spatiotemporal intermittency seen at $\Omega = 0.06, \epsilon = 0.7928$ (one of the points marked with diamonds in Fig. 1), and (b) spatial intermittency seen at $\Omega = 0.047, \epsilon = 0.336$ (marked with asterisk in Fig. 1). The index i represents the lattice sites and the index t represents time.

hibiting regular temporal behavior, and turbulent states with irregular temporal behavior, can be identified near the bifurcation boundary of spatiotemporally fixed point solutions in the phase diagram. The spatiotemporal intermittency seen in the spreading regime has been shown to belong to the directed percolation class. In the non-spreading regime, a different class of intermittency called the spatial intermittency is seen near the bifurcation boundary. We discuss these two classes of intermittency briefly in the following sections.

A. Spatiotemporal intermittency of the DP class and the spreading regime

Spatiotemporal intermittency belonging to the directed percolation class is seen in the vicinity of the bifurcation boundary of the spatiotemporally fixed point solutions in the spreading regime [9, 10, 11]. Some of the points that show this kind of spatiotemporal intermittency have been marked with diamonds (\diamond) in the phase diagram (Fig. 1). In this type of intermittency, the fixed point solution of the single sine circle map, x^* acts as the laminar state, whereas the burst states lie in the $[0, 1]$ interval. Since burst states cannot be spontaneously created, the laminar state acts as an absorbing state. The burst states can either 'percolate' through the lattice by infecting a neighboring laminar state, or die down to the laminar state. With time acting as the directed axis, the analogy with directed percolation is complete. Moreover, this class of spatiotemporal intermittency is remarkably free of coherent structures, some times called 'solitons', which spoil the analogy

	Ω	$\epsilon_c(\Omega)$	Static exponents					Spreading Exponents		
			z	$\beta/\nu z$	β	η'	ζ	η	δ	z_s
STI-DP	0.060	0.7928	1.59(0.02)	0.17(0.02)	0.293	1.51(0.01)	1.68(0.01)	0.315(0.007)	0.16(0.01)	1.26(0.01)
	0.065	0.34949	1.59(0.03)	0.16(0.01)	0.273	1.50(0.01)	1.66(0.01)	0.303(0.001)	0.16(0.01)	1.27(0.01)
	DP		1.58	0.16	0.28	1.51	1.67	0.313	0.16	1.26
SI	0.04	0.402	-	-	-	-	1.10(0.04)	-	-	-
	0.047	0.336	-	-	-	-	1.13(0.02)	-	-	-

TABLE I: The static and dynamic (spreading) exponents (see [9, 10] for definitions) obtained at two of the directed percolation (DP) points (\diamond -s) in Figure 1 are shown in the first two rows of the table. The universal DP exponents are listed in the third row. The laminar length distribution exponent, ζ , calculated for spatial intermittency (SI) at two points marked by (Δ -s (quasi-periodic bursts) and ($*$ -s (periodic bursts) respectively in Fig. 1, are also listed. The error-bars are shown in the brackets. The data has been obtained for a lattice of size, $N = 10^3$ and has been averaged over 10^3 initial conditions. The laminar length distributions have been calculated for a lattice of size $N = 10^4$ and averaged over 50 initial conditions.

with directed percolation in other models such as the Chaté Manneville coupled map lattice [3].

An entire set of static and dynamic scaling exponents was obtained in this parameter regime, which showed good agreement with the universal DP exponents. The exponents obtained, after averaging over 10^3 initial conditions, at two such parameter values are listed in Table I. Similar exponents have been seen at points marked with diamonds (\diamond) in the phase diagram (Figure 1). These exponents also satisfy the hyperscaling relations for the static exponents ($2\beta/\nu = d - 2 + \eta'$), and the spreading exponents ($4\delta + 2\eta = dz_s$) for $d = 1$. Hence, this class of spatiotemporal intermittency seen at the bifurcation boundary in the spreading regime belongs convincingly to the directed percolation class. These scaling exponents are however, seen only near the bifurcation boundary. The distribution of laminar lengths for the spreading solutions off the bifurcation boundary, show an exponential fall off. Thus STI of the DP class is a special case of the spatiotemporal behavior seen in the spreading regime.

A different class of intermittency is seen below the infection line, i.e in the non-spreading

regime. This is the phenomenon of spatial intermittency.

B. Spatial intermittency and the non-spreading regime

Below the infection line, in the non-spreading regime, the laminar sites are the synchronized fixed point x^* and the burst sites are either temporally frozen, periodic or aperiodic. These bursts are very stable and do not die down with time.

In the vicinity of the bifurcation boundary, a special class of intermittency called spatial intermittency is seen. In this case, the temporal behavior of the burst states is either quasi-periodic or periodic. Some of these points have been marked with triangles (Δ , quasi-periodic) and asterisks (*, periodic) in the phase diagram (Fig. 1). In this class of intermittency, the distribution of laminar lengths, obtained by averaging over different random initial conditions, scales as a power-law of the form $P(l) \sim l^{-\zeta}$, with ζ as the associated scaling exponent [11]. The exponent ζ obtained in this case was found to be ~ 1.1 (Table I). A similar scaling exponent has been seen in the case of the spatial intermittency observed in inhomogeneous logistic map lattice [13]. The laminar length distributions seen for other non-spreading solutions at points off the bifurcation boundary show an exponential decrease. Thus the spatially intermittent solutions are special cases of the solutions in the non-spreading regime.

Thus the sine circle coupled map lattice shows a transition from a spreading regime to a non-spreading regime at the infection line. In order to gain further insights into this transition, we map the coupled map lattice to a stochastic model, a probabilistic cellular automaton of the Domany-Kinzel type [3, 14].

III. MAPPING TO AN EQUIVALENT CELLULAR AUTOMATON

Signatures of the spreading to non-spreading transition at the infection line are seen in a mapping of the coupled map lattice to a stochastic model namely, a probabilistic cellular automaton of the Domany-Kinzel type [3, 14]. The equivalent cellular automaton, set up to mimic the dynamics of the laminar and burst states in the coupled map lattice defined in eq. 1, is defined on a one dimensional lattice of size N . The state variable v_i^t at site i and at time t is assigned the value $v_i^t = 0$ if the site is in the laminar state, and $v_i^t = 1$ if the site

is in the burst state.

As in the coupled map lattice equation 1, the probability of the site i at time $t + 1$ being in the burst state depends on the state of the sites $i - 1, i$ and $i + 1$ at time t . We therefore define the cellular automaton dynamics in this system by the conditional probability $P(v_i^{t+1}|v_{i-1}^t, v_i^t, v_{i+1}^t)$. There are 2^3 possible configurations and the symmetry between the sites $i - 1$ and $i + 1$ in equation 1 gives the effective probabilities p_k 's as $p_0 = P(1|000)$, $p_1 = P(1|001) = P(1|100)$, $p_2 = P(1|010)$, $p_3 = P(1|011) = P(1|110)$, $p_4 = P(1|101)$ and $p_5 = P(1|111)$. These probabilities then define the update rules of the cellular automaton.

We estimate these probabilities p_k , for a given set of parameter values, from the numerical evolution of the coupled map lattice with random initial conditions. The probabilities p_k 's are calculated by finding the fraction of sites i which exist in the burst state $v_i^{t+1} = 1$ at time $t + 1$, given that the site i and its nearest neighbors $i - 1$ and $i + 1$ existed in state k at time t . That is, the probability p_k is determined using $p_k = \frac{N_1^k}{N_0^k + N_1^k}$, where N_0^k and N_1^k are the number of sites, which at time t were the central sites of the configuration k , and at time $t + 1$ exist in the laminar states ($v_i^{t+1} = 0$) and the burst states ($v_i^{t+1} = 1$) respectively. These probabilities, were extracted from a coupled map lattice of size $N = 10^3$ averaged over 14000 time steps discarding a transient of 1000 time steps, and averaged over 200 initial

	Ω	ϵ	p_0	p_1	p_2	p_3	p_4	p_5
S(DP)	0.060	0.7928	0.0	0.220	0.0	0.933	0.627	0.984
	0.073	0.4664	0.0	0.150	0.0	0.938	0.439	0.993
S	0.070	0.264	0.0	0.140	0.0	0.982	0.391	0.999
		0.248	0.0	0.050	0.0	0.989	0.160	0.999
NS	0.070	0.232	0.0	0.000	0.0	1.000	0.000	1.000
		0.228	0.0	0.000	0.0	1.000	0.000	1.000
NS(SI)	0.031	0.420	0.0	0.000	0.0	1.000	0.000	1.000
	0.044	0.373	0.0	0.000	0.0	1.000	0.000	1.000

TABLE II: shows the probabilities p_k 's obtained in the spreading (S), non-spreading (NS) regimes and at directed percolation (DP) and spatial intermittency (SI) points.

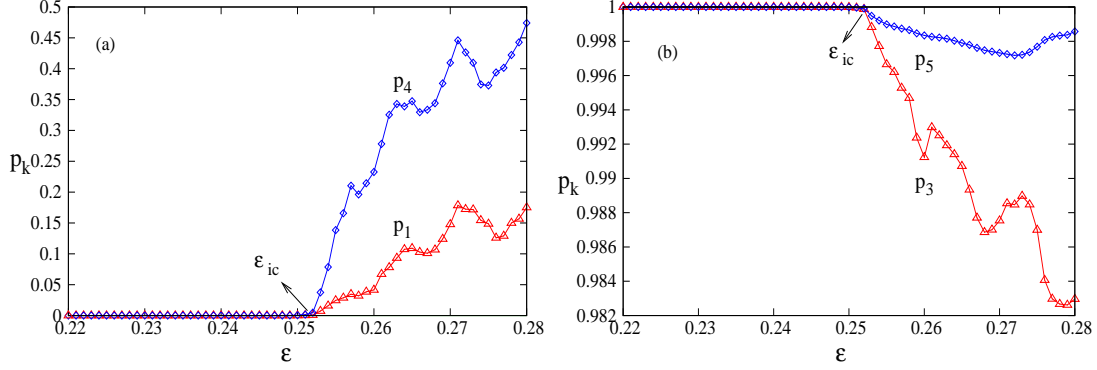


FIG. 3: (Color online) shows the probabilities associated with the update rules p_1, p_3, p_4, p_5 plotted as a function of the coupling strength, ϵ at $\Omega = 0.065$. In the non-spreading regime ($\epsilon < \epsilon_{ic}$), the probabilities are either 0 or 1, whereas they lie in the interval $(0, 1)$ in the spreading regime ($\epsilon \geq \epsilon_{ic}$).

conditions. The probabilities p_k obtained in the spreading and non-spreading regimes in the phase diagram are listed in Table II.

It is clear that the condition for an absorbing state is realized in the probability $p_0 = P(1|000)$ which is seen to be zero in both regimes. The probabilities $p_1 = P(1|001) = P(1|100)$ and $p_4 = P(1|101)$ essentially define infection probabilities, which estimate the probability of a laminar site being infected by its burst neighbor or neighbors, to change to a burst site.

We can see from Table II that these probabilities show drastically different behavior in the spreading and non-spreading regimes. In the case of the spreading regime, the probabilities obtained are seen to lie in the open interval $(0, 1)$. Therefore, the dynamics in the spreading regime is described by a probabilistic cellular automaton (PCA) wherein the cellular automaton rules are probabilistic in nature. In contrast, in the case of the non-spreading regime, in addition to p_0 and p_2 which are zero for the STI of the DP type [15], the infection probabilities p_1 and p_4 are also seen to be equal to zero. Hence, the infection probabilities characterize the non-infective nature of the bursts. Moreover, the probabilities $p_3 = P(1|011) = P(1|110)$ and $p_5 = P(1|111)$ take the value 1, which indicates the robustness of the burst states. We note that the probabilities obtained here only take the values 0 or 1. Hence, we obtain a deterministic cellular automaton (DCA) in the non-spreading regime, wherein given a state k at time t , the state of the site i at time $t + 1$ is decisively known with

probability zero or one. This is further illustrated in Figure 3, where the probabilities have been plotted as a function of the coupling strength ϵ at $\Omega = 0.065$. The probabilities show a distinct change to values other than zero or one, at the point where spreading regime starts viz. $\epsilon > \epsilon_{ic}$ (See inset in Fig. 1). Thus a transition from a probabilistic to a deterministic cellular automaton is seen at the infection line.

It is therefore clear that the spatiotemporal intermittency of the directed percolation class seen in the spreading regime can be modeled by a PCA, whereas spatial intermittency observed in the non-spreading regime can be modeled by a DCA. In the following section, we show that the probabilistic cellular automata obtained at the STI of the DP points indeed mimics the dynamics of the coupled map lattice and shows scaling exponents matching with the universal directed percolation exponents.

A. Probabilistic cellular automaton and directed percolation

As mentioned previously, the dynamics seen in the case of spatiotemporal intermittency in the spreading regime resembles that of directed percolation. The stochastic nature of the burst states is further emphasized in the probabilistic cellular automaton obtained in this regime. In this section, we show that the probabilistic cellular automata obtained at points in the phase diagram which show DP-like spatiotemporal intermittency, indeed show scaling behavior which match with the directed percolation class.

Figure 4 shows some of the physical quantities associated with the static and dynamical properties of the system. The scaling exponents obtained for these quantities are also shown in the figure. The probabilities associated with the PCA obtained at the parameter value $\Omega = 0.06, \epsilon = 0.7928$, were found to be $p_0 = 0.0, p_1 = 0.213116, p_2 = 0.000081, p_3 = 0.902515, p_4 = 0.569464$ and $p_5 = 0.967595$. When the cellular automaton is prepared with random initial conditions, such that the sites take either 0 or 1 values with equal probabilities at time $t = 0$, the burst state (1 state) is seen to die down with time. The relaxation time τ , which determines the time taken by the lattice to relax to a laminar state (0 state), scales as a function of the size of the lattice L as $\tau \sim L^z$ (Fig. 4(a)). The order parameter m , defined as the fraction of burst sites in the lattice, decreases with time as $m \sim t^{-\beta/\nu z}$ (Fig. 4(b)). In contrast, when a pair of burst states are introduced in a lattice prepared in the laminar state at time $t = 0$, the burst states are seen to grow with time. The dynamical quantities

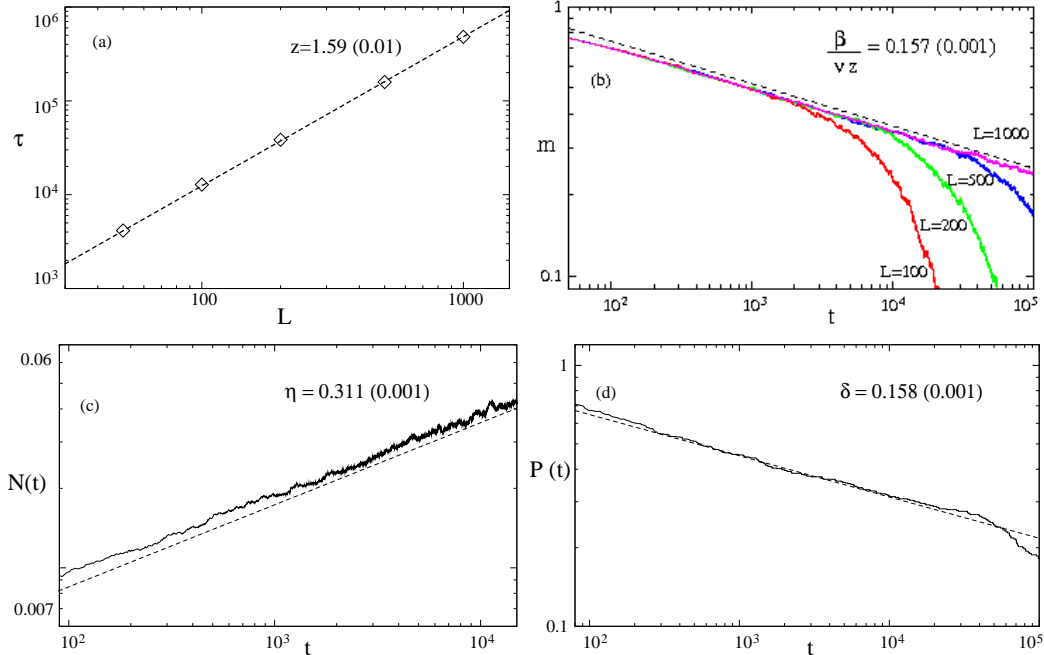


FIG. 4: (Color online) shows the log-log (base 10) plot of physical quantities calculated for the probabilistic cellular automaton associated with the DP point $\Omega = 0.06, \epsilon = 0.7928$. The figure shows the (a) escape time τ vs length of the lattice L , (b) order parameter m vs time t , and the spreading properties (c) the fraction of burst sites $N(t)$ vs t , and (d) the survival probability $P(t)$ plotted as a function of time t . The fits to the plots and the corresponding scaling exponents (error bars in brackets) obtained are also shown.

associated with the growth of the burst states viz. the fraction of burst sites $N(t)$, and the survival probability $P(t)$, which is defined as the fraction of initial conditions which yield a non-zero number of burst states at time t , are shown in Fig. 4(c) and (d). The respective scaling exponents obtained show good agreement with the directed percolation class. Thus the cellular automaton model obtained in the region of spatiotemporal intermittency seen in the spreading regime exhibits scaling behavior similar to the directed percolation class, as expected.

We note that in the case of the non-spreading regime, the deterministic cellular automaton obtained acts like an identity mapping. Therefore, the scaling behavior in the laminar length distribution depends strongly on the initial condition namely, the fraction of burst states in the lattice. To mimic the dynamics exhibited by the coupled map lattice, we calculate the fraction of burst sites in a coupled map lattice of size 20000 at $\Omega = 0.04, \epsilon = 0.402$,

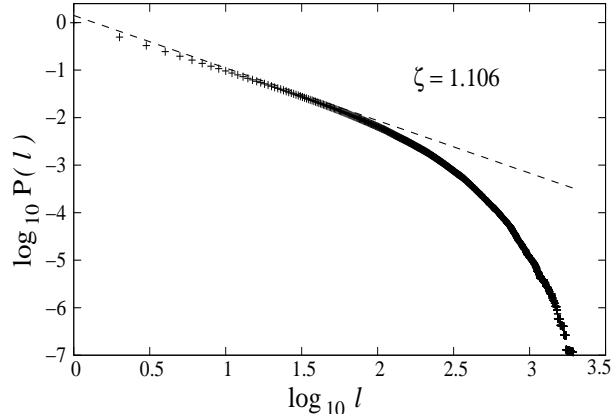


FIG. 5: shows the laminar length distribution obtained for the deterministic cellular automaton obtained at the spatial intermittency point $\Omega = 0.04, \epsilon = 0.402$. The exponent obtained is $\zeta = 1.106 \pm 0.005$.

after discarding 60000 transients and averaging over 50 random initial conditions. The fraction of burst sites came out to be $p = 0.0684$. Fig. 5 shows the scaling behavior of the distribution of laminar lengths for the deterministic cellular automaton, obtained for this initial condition, in which bursts were introduced with probability p . The exponent seen in the cellular automaton turns out to have the value $\zeta \sim 1.1$ as in the coupled map lattice.

A mean-field study of the cellular automaton gives further insights into the transition from probabilistic to deterministic cellular automaton, as well as into the initial condition dependence of the cellular automata. We discuss this in the subsequent section.

B. Mean-field analysis of the cellular automaton

We study a mean field approximation of the probabilistic cellular automaton which gives a better understanding of the probabilistic to deterministic cellular automaton transition as well as gives probability bounds for the directed percolation-like behavior [16]. Let m_t and m_{t+1} be the density of burst states in the lattice at the t^{th} and $t + 1^{th}$ time step. The mean-field for the probabilistic cellular automaton can be defined, according to the cellular automaton rules, as

$$m_{t+1} = (2p_1 + p_2)m_t(1 - m_t)^2 + (2p_3 + p_4)m_t^2(1 - m_t) + p_5m_t^3 \quad (2)$$

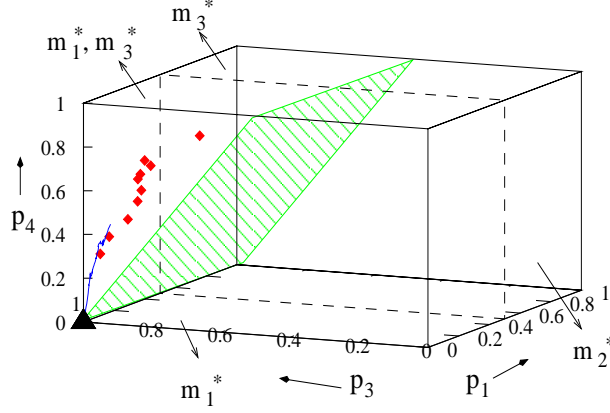


FIG. 6: (Color online) shows the stability regions of the three fixed points of the mean-field equation 3, m_1^* , m_2^* , and m_3^* , in the $\{p_1, p_3, p_4\}$ phase space. The probabilities of the DP points (marked with diamonds), as well as for points in the spreading regime at $\Omega = 0.065$ (dotted line) have been shown. The triangle corresponds to the probabilities in the non-spreading regime.

By approximating $p_5 = 1$ and $p_2 = 0$, the mean field equation reduces to

$$m_{t+1} = 2p_1 m_t(1 - m_t)^2 + (2p_3 + p_4) m_t^2(1 - m_t) + m_t^3 \quad (3)$$

The three fixed points of this equation for a set of parameters $\{p_1, p_3, p_4\}$ are $m_1^* = 0$, $m_2^* = \frac{2p_1 - 1}{1 + 2p_1 - 2p_3 - p_4}$, and $m_3^* = 1$. A linear stability analysis of the mean-field equation indicates that the fixed point $m_1^* = 0$, which corresponds to the absorbing state, is stable when $p_1 < \frac{1}{2}$. The fixed point m_2^* is stable when $2p_3 + p_4 \leq 2$ and $2p_1 \geq 1$. The fixed point $m_3^* = 1$, which corresponds to the completely turbulent state, is stable when $2p_3 + p_4 \geq 2$. The stability regions of these three fixed points in the $\{p_1, p_3, p_4\}$ space have been indicated in Fig. 6. The $2p_3 + p_4 = 2$ plane, above which $m_3^* = 1$ solutions are found to be stable, is shown in the figure.

We see that both $m_1^* = 0$ and $m_3^* = 1$ solutions are stable, when $p_1 \leq \frac{1}{2}$ and $2p_3 + p_4 \geq 2$. This is the co-existence region. The system settles down to either the completely laminar state ($m_1^* = 0$) or the completely turbulent state ($m_3^* = 1$) in the co-existence region, depending on the initial condition m_t at $t = 0$. The solutions settle down to the $m_1^* = 0$ solution if initial density, $m_0 \in [0, m_2^*)$ whereas, they tend towards $m_3^* = 1$ if $m_0 \in (m_2^*, 1]$. For instance, we iterate the map equation 3 by choosing $p_4 = 0.9$ and study the $\{m, p_1, p_3\}$

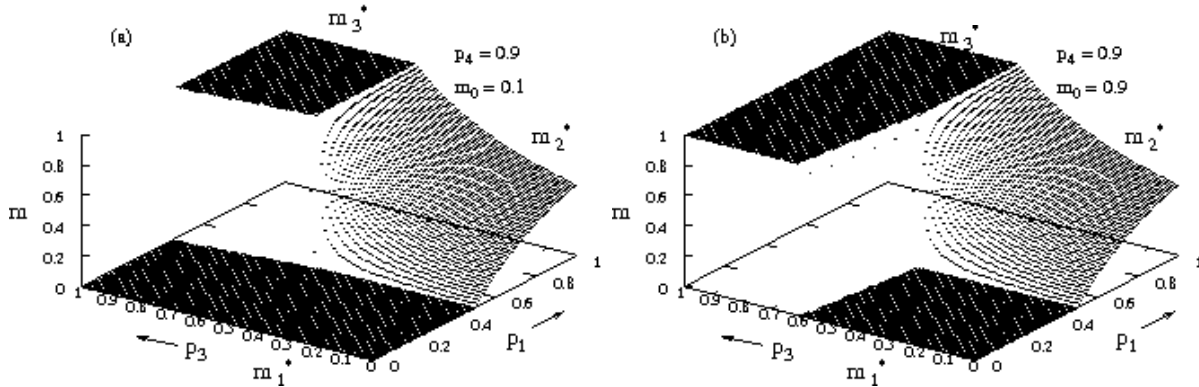


FIG. 7: shows the $\{m, p_1, p_3\}$ phase diagram of the mean field map at $p_4 = 0.9$ with initial m at time $t = 0$ chosen as (a) $m_0 = 0.1$ and (b) $m_0 = 0.9$. In the co-existence region ($2p_3 \geq 1.1$ and $p_1 \leq 0.5$), the density of burst sites m , settles down to either m_1^* or m_3^* depending on the initial density m_0 chosen.

phase diagram for two initial conditions $m_0 = 0.1$ and $m_0 = 0.9$. The $\{m, p_1, p_3\}$ phase diagram obtained is shown in Figure 7(a) and (b) respectively. We see that the solutions settled down to $m^* = 0$ in the co-existence region in the first case, whereas they settle down to $m^* = 1$ in the latter case. Hence, the solutions in the co-existence region are initial condition dependent.

Interestingly, we find that the probabilities associated with the spreading regime of the coupled map lattice, including those obtained for the directed percolation points in the spreading regime, lie in the co-existence region (Figure 6). Due to this, the probabilistic cellular automaton has a very strong initial condition dependence in the spreading region. The correct choice of initial conditions leads to the laminar absorbing state. Other choices can end up easily in the $m = 1$ state. However, the points at which directed percolation is seen are exceptions to this. The probabilistic cellular automata obtained at these points show scaling behavior consistent with the directed percolation phenomena irrespective of the choice of initial conditions, as was discussed in the previous section.

The probabilities associated with the deterministic cellular automaton seen in the non-spreading regime (i.e. $p_1 = 0$, $p_3 = 1$, $p_4 = 0$) lie at the vertex belonging to the co-existence region in this cube. This point has been marked with a triangle in Figure 6. As we approach the spatial intermittency points along the bifurcation boundary, the cellular automaton probabilities obtained at the directed percolation points tend towards this vertex. Similarly,

the probabilities obtained in the spreading regime tend towards this vertex, as we cross the infection line and enter the non-spreading regime. Therefore, the deterministic cellular automaton is a limiting case of the probabilistic cellular automaton seen in the spreading regime.

This confirms that the presence of both spreading and non-spreading regimes separated by the infection line in the phase diagram, which accounts for the presence of both directed percolation-like spatiotemporal intermittency and spatial intermittency in the phase diagram, is manifested in the form of a transition from probabilistic to deterministic cellular automaton at the infection line. However, the origins of the spreading nature of the burst states above the infection line are not clear. In the next section, we identify the dynamical origins of the spreading states.

IV. CRISIS AND UNSTABLE DIMENSION VARIABILITY AT THE INFECTION LINE

It is clear from the preceding discussion that the behavior of the burst states changes drastically at the infection line leading to the spreading to non-spreading transition and the existence of distinct classes of spatiotemporal intermittency in the phase diagram. We now have indications that the origin of the spreading states lies in an attractor-widening crisis at the infection line as well as the presence of unstable dimension variability in the vicinity of the infection line, as we will see in this section.

A crisis is said to have occurred in a dynamical system when a sudden change in the attractor takes place when a system parameter is changed [17]. We observe such a phenomenon in our coupled map lattice, when we change the strength of the coupling between sites, ϵ , for a given Ω in the vicinity of the infection line. This has been illustrated in Fig. 8. Here, the variable x associated with a typical site has been plotted over 500 time steps, as a function of the coupling strength ϵ at $\Omega = 0.065$.

The range of ϵ values on the vertical axis of Fig. 1 cuts across the infection line at $\epsilon_{ic} = 0.252$ for $\Omega = 0.065$. The bifurcation diagram clearly shows that an attractor widening crisis [18] appears at this point. Similar behavior is seen for other sites. The spreading regime seen in the phase diagram emerges exactly at the point at which the attractor widens, with the non-spreading regime corresponding to the pre-widening regime. This widening also

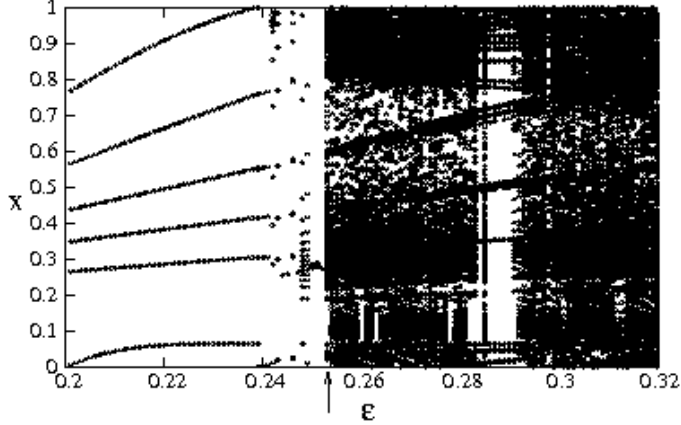


FIG. 8: shows the bifurcation diagram of the coupled map lattice in which the variable x associated with a typical site has been plotted over 500 time steps, as a function of the coupling strength ϵ in the neighborhood of the infection line, at $\Omega = 0.065$.

identifies the point at which the equivalent cellular automaton undergoes a probabilistic to deterministic transition. In the pre-crisis region, each site follows either a periodic or quasi-periodic trajectory and is not infected by the behavior of its neighbors. Thus, its CA analogue is deterministic as listed in Table II. In the post-crisis regime, each site is able to access the full x range, as well as infect its neighbors, and the bursting and spreading behavior characteristic of the spreading regime is seen. This is reflected in the equivalent cellular automaton by a transition to probabilistic behavior (Table II). It is to be noted that the volume of the attractor in phase space will be much larger post-crisis, as compared to the pre-crisis volume.

We also see indications of unstable dimension variability in the vicinity of the infection line. An attractor is said to have unstable dimension variability, if it possesses periodic orbits with different number of stable and unstable directions [19, 20]. A trajectory visiting the neighborhood of these periodic orbits, experiences a fluctuating number of unstable directions, as time progresses. A signature of this phenomenon can be seen in the finite time Lyapunov exponents (FTLE) of the system which fluctuate about zero, as the dynamics evolves.

For the coupled map lattice of eq. 1, which is an N -dimensional map of the form $\mathbf{x} \rightarrow \mathbf{f}(\mathbf{x})$, let the Jacobian evaluated at the initial condition \mathbf{x}_0 be denoted as $\mathbf{Df}(\mathbf{x}_0)$. The time- n Lyapunov exponents (FTLE) for this system, are obtained by diagonalizing the Jacobian

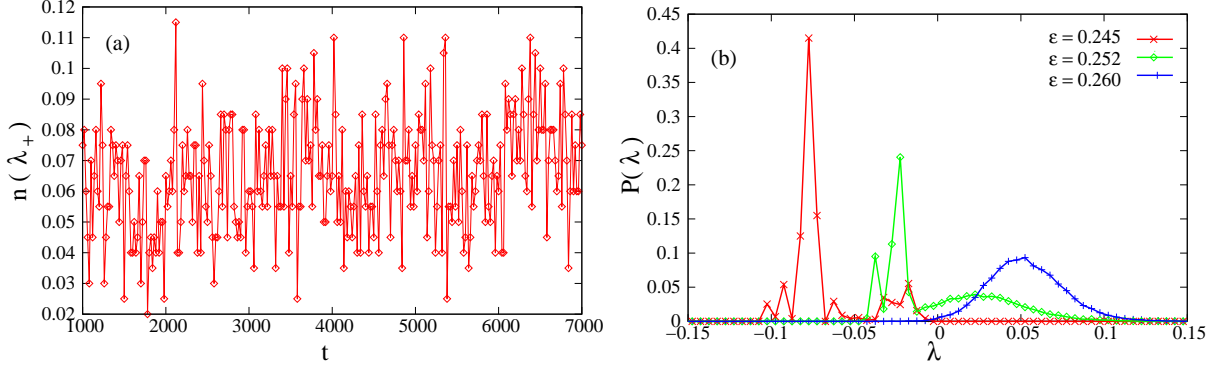


FIG. 9: (Color online) shows (a) the fraction of positive finite-time Lyapunov exponents (time=20) as a function of time t obtained at $\Omega = 0.065, \epsilon = 0.254$, and (b) the distribution of the largest finite-time Lyapunov exponent (time= 100) plotted for $\Omega = 0.065$ and $\epsilon = 0.245, 0.252, 0.260$.

$\mathbf{Df}^n(\mathbf{x}_0)$ of the n -times iterated map \mathbf{f}^n , the k^{th} time- n Lyapunov exponent being defined as

$$\lambda_k(\mathbf{x}_0, n) = \frac{1}{n} \log \Lambda_k \quad (4)$$

where, Λ_k is the k^{th} eigenvalue of the time- n Jacobian $\mathbf{Df}^n(\mathbf{x}_0)$.

We find that the finite-time Lyapunov exponents obtained for our system exhibit fluctuations about zero in the vicinity of the infection line. This can be seen in Fig. 9(a), where the fraction of positive time-20 Lyapunov exponents obtained at $\Omega = 0.065, \epsilon = 0.254$, is plotted as a function of time. The fraction of positive exponents is seen to vary with time, indicating that a fraction of the Lyapunov exponents fluctuate about zero, as the dynamics evolves. Hence, the trajectory of the coupled map visits periodic orbits with different number of unstable directions, in the vicinity of the infection line.

This is further illustrated in Fig. 9(b), which shows the distribution of the largest time-100 Lyapunov exponent, obtained at $\Omega = 0.065$ for various values of ϵ . The distribution has been calculated by collecting data for a lattice of size $N = 200$ over 10000 time steps and by averaging over 200 initial conditions. We find that the distribution of the largest time-100 Lyapunov exponent is constrained to the negative values for parameters lying in the non-spreading regime (eg. $\epsilon = 0.245$ in Fig. 9(b)). For parameters close to the infection line (viz. $\epsilon = 0.252$), the distribution shifts towards the positive side, until it lies entirely in the positive side of the axis for parameters above the infection line (eg. $\epsilon = 0.260$). Hence, the distribution of Lyapunov exponents obtained at $\epsilon = 0.252$ illustrates further that the

largest finite-time Lyapunov exponent vacillates around zero near the infection line.

Therefore, we infer from Fig. 9(a) and (b), that the finite-time Lyapunov exponents fluctuate about zero, near the infection line, thereby confirming the presence of unstable dimension variability at the infection line. Hence, we see that the spreading nature of the bursts above the infection line can be attributed to the attractor-widening crisis as well as the presence of unstable dimension variability at the infection line.

V. DISCUSSION

To conclude, the spatiotemporal intermittency of the directed percolation class and the spatial intermittency of the non-directed percolation class, seen along the bifurcation boundaries of spatiotemporally fixed point solutions, are special cases of the spreading and non-spreading regimes seen off the bifurcation boundaries. The two regimes are separated by the infection line which intersects with the bifurcation boundary of the fixed point solutions at the point where the cross-over between the directed percolation and non-directed percolation behavior takes place. Thus the behavior seen in coupled sine circle map lattice is organized around the locations of the bifurcation boundaries of the fixed point solutions, and the infection line. The existence of two distinct universality classes, in the phase diagram of the sine circle map lattice is reflected in the transition of the equivalent cellular automaton from the probabilistic phase to the deterministic phase and the concomitant suppression of the spreading or infectious modes. The dynamic origins of this transition lie in an attractor-widening crisis. We also find evidence for the existence of unstable dimension variability in the neighborhood of the infection line. Thus, in this system, there is a direct connection between a dynamical phenomenon viz. a crisis in an extended system and the statistical properties of the extended system viz. the exponents and universality classes. Similar directed percolation to non-directed percolation transitions have been seen in other coupled map lattices, as well as in pair contact processes, solid on solid models and models of non-equilibrium wetting [21]. Our results may have useful pointers for the analysis of other systems, and thus contribute to the on-going debate on the identification of the universality classes of spatiotemporal systems.

Acknowledgment: NG thanks DST, India for partial support under the project

- [1] F. Daviaud, M. Bonetti and M. Dubois, Phys. Rev. A. **42**, 3388 (1990); P. W. Colovas and C. D. Andereck, Phys. Rev. E. **55**, 2736 (1997); M. Das, B. Chakrabarti, C. Dasgupta, S. Ramaswamy and A.K. Sood, Phys. Rev. E. **71**, 021707 (2005); C. Pirat, A. Naso, J.L Meunier, P. Massa and C. Mathis, Phys. Rev. Lett. **94**, 134502 (2005).
- [2] Y. Pomeau, Physica D. **23**, 3 (1986).
- [3] H. Chaté and P. Manneville, Physica D **32**, 409 (1988).
- [4] P. Grassberger and T. Schreiber, Physica D, **50**, 177 (1991).
- [5] T. Bohr, M. van Hecke, R. Mikkelsen, M. Ipsen Phys. Rev. Lett. **86** 5482 (2001).
- [6] J. Rolf, T. Bohr, and M. H. Jensen, Phys. Rev. E **57**, R2503 (1998).
- [7] P. Rupp, R. Richter and I. Rehberg, Phys. Rev. E. **67**, 036209 (2003).
- [8] K.A. Takeuchi, M. Kuroda, H. Chaté, and M. Sano, Phys. Rev. Lett **99**, 234503 (2007).
- [9] T.M. Janaki, S. Sinha, and N. Gupte, Phy. Rev. E **67**, 056218 (2003).
- [10] Z. Jabeen and N. Gupte, Phys. Rev. E **72**, 016202(2005).
- [11] Z. Jabeen and N. Gupte, Phys. Rev. E **74**, 016210(2006).
- [12] G. Pradhan, N. Chatterjee, and N. Gupte, Phys. Rev. E **65**, 046227 (2002).
- [13] A. Sharma and N. Gupte, Phys. Rev. E **66**, 036210 (2002).
- [14] E. Domany and W. Kinzel, Phys. Rev. Lett. **53**, 311 (1984).
- [15] The probability $p_2 = P(1|010)$ is also seen to be equal to zero in both the regimes, though the reasons are different. In the spreading regime, we find that the neighboring laminar states suppress the central burst state, and hence we obtain a zero probability for p_2 . In the case of the non-spreading regime, a single burst site with two laminar neighbors is never observed.
- [16] A similar study has been carried out in F. Bagnoli *et al*, Phys. Rev. E. **63**, 046116 (2001), in which the probability rules were defined differently.
- [17] C. Grebogi, E. Ott, and J.A. Yorke, Phys. Rev. Lett. **48**, 1507 (1982).
- [18] C. Grebogi, E. Ott, F. Romeiras, and J.A. Yorke, Phys. Rev. A **36**, 5365 (1987).
- [19] E.J. Kostelich, I. Kan, C. Grebogi, E. Ott, and J.A. Yorke, Physica D **109**, 81 (1997).
- [20] Y.C. Lai, C. Grebogi and J. Kurths, Phys. Rev. E **59**, 2907 (1999); Y.C. Lai, D. Lerner, K. Williams, and C. Grebogi, Phys. Rev. E **60**, 5445 (1999).

[21] G. Odor, Rev. Mod. Phys. **76**, 663, (2004).